Annu. Rev. Phys. Chem. 1990. 41:647–81

FEMTOSECOND OPTICAL SPECTROSCOPY: A Direct Look at Elementary Chemical Events

Shaul Mukamel[1]

Chemistry Department, University of Rochester, Rochester, New York 14627

KEY WORDS: nonlinear spectroscopy, pump-probe and hole burning, density matrix, quantum beats, femtosecond CARS.

INTRODUCTION

Ultrafast optical spectroscopy using laser pulses as short as 6 femtoseconds provides a novel probe for molecular nuclear motions (1, 2). Since the duration of such pulses is comparable to or shorter than typical molecular vibrational periods (10 fsec is the period of a 3300 cm^{-1} vibration), these pulses make it possible to probe molecular vibrations and elementary photophysical and photochemical events in real time. Femtosecond dynamics and relaxation studies have been carried out in solutions (3–9a,b), neat liquids (10–13), conjugated polymers (14–15), proteins and biological systems (16–17), crystals (18a–c), surfaces (19a,b), semiconductors (20–21), molecular aggregates (22–23), the hydrated electron (24a–c), isolated molecules in supersonic beams (25–26), and the gas phase (27a,b). Femtosecond nonlinear optical measurements have numerous unique advantages. Consider, for example, the simplest ultrafast spectroscopic technique: pump-probe spectroscopy (4–6, 25a–c). In this technique the system is subjected to two short pulses separated by a time delay τ. The first pulse (the pump pulse) has a frequency ω_1 and the absorption of

[1] Camille and Henry Dreyfus Teacher/Scholar.

0066–426X/90/1101–0647$02.00

the second pulse (the probe pulse) with frequency ω_2 is monitored as a function of ω_1, ω_2, τ, and the pulse durations. Ideally we would like to think of this technique as "snapshot" spectroscopy with the following intuitive picture: The pump pulse prepares the system in a nonequilibrium state denoted the *doorway state*. This state then propagates for a time τ. The probe pulse subsequently measures this state by providing a *window*, which depends on ω_2. The ability to control τ and ω_2 allows us to probe the system at the right moment and in the right place. In a photoisomerization or photodissociation process the system spends only a short time in the transition state. Femtosecond spectroscopy allows the observation of these dynamics through a window that opens up at the moment of interest, and offers a uniquely sensitive and accurate technique for the measurement of chemical dynamics. In addition, by using properly timed and tuned multiple pulse sequences with controlled shapes and phases (28a–c), it may become possible to optically prepare a molecular system at a desired region of phase space that would not otherwise be accessible with use of linear optics and its selection rules. This could result in laser control of chemical reactivity (29–30). Coherent nonlinear optical techniques other than pump-probe spectroscopy, such as coherent Raman spectroscopy (31–32), transient gratings (33, 34a,b), photon echoes (8a,b, 35, 36a–c), and four wave mixing (14a,b, 35, 36a–c), simply differ by the choice of wavevectors, frequencies, and timing of the various laser pulses.

There are several major challenges in the quantitative interpretation of these experiments. For sufficiently simple systems with a few degrees of freedom, an exact fully quantum treatment is feasible. For example, the supersonic beam ICN photodissociation and NaI curve crossing pump-probe experiments (25a–c) have triggered a considerable amount of theoretical activity (37–43), focused on solving the one dimensional Schrödinger equation for the time dependent wavefunction. More complicated situations (larger systems and condensed phase measurements) require the introduction of statistical methods. Phenomenological formulations based on the multilevel Bloch equations (44–45) or a driven oscillator model (46a,b) are often used to interpret experimental data in condensed phases.

In this review I present a unified description of nonlinear spectroscopic techniques based on the density matrix (47a–c). Formulating the problem by using the density matrix and its evolution in Liouville space offers a natural and simple way to treat nonlinear optical spectroscopies; additionally, this formulation allows the selective elimination of inessential "bath" degrees of freedom, the carrying out of thermal averagings, and the development of a mixed quantum and classical description of different degrees of freedom. In the density matrix description the various interactions with the radiation field are fully time ordered, and the relationships among the numerous time domain and frequency domain spectroscopies and their information content are clarified. I first introduce the nonlinear polarization and show how the density matrix provides the natural bookkeeping for the various interactions. I then specialize to pump-probe spectroscopy and discuss the limitations of the intuitive "snapshot" picture (26a,b, 48, 49). General conditions under which this picture holds are precisely defined and several extensions are given. I next introduce a multimode Brownian oscillator model for polyatomic molecules (50) that accounts for coherent vibrations, solvent modes, spectral diffusion, and homogeneous and inhomogeneous line broadening. The hole-burning and photon echo are two resonant techniques that have the capacity of eliminating inhomogeneous broadening and extracting useful dynamical information out of structureless lineshapes (35, 36a–c, 51–53). I analyze these techniques as well as off resonant Raman scattering spectroscopies, which in the impulsive limit show femtosecond quantum beats.

DYNAMICS OF THE MOLECULAR DENSITY MATRIX: THE EIGHTFOLD WAY FOR THE NONLINEAR RESPONSE FUNCTION

Here I consider a molecular system with three electronic states: a ground state $|g\rangle$ and two excited states $|e\rangle$ (an intermediate electronic state) and $|f\rangle$ (the upper excited electronic state). The molecular Hamiltonian is (48)

$$H = |g\rangle H_g\langle g| + |e\rangle H_e\langle e| + |f\rangle H_f\langle f|. \qquad 1.$$

The adiabatic Hamiltonians H_v ($v = g, e,$ or f) describe the nuclear motions of the molecule as well as other nuclear degrees of freedom (solvent, matrix host, etc). The 0–0 electronic transition energies will be denoted ω_{eg} (for the $|g\rangle$ to $|e\rangle$ transition) and ω_{fe} (for the $|e\rangle$ to $|f\rangle$ transition). The dipolar interaction of the system with an external electromagnetic field, $E(\mathbf{r}, t)$ is $H_{\text{int}} = -\mu E(\mathbf{r}, t)$, μ being the molecular electronic transition dipole operator, which couples states $|g\rangle$ to $|e\rangle$ and $|e\rangle$ to $|f\rangle$. I shall consider μ and E to be scalar quantities. Their vector nature is important when studying orientational effects, which can be detected by varying the polarization of the light fields (2, 9a,b, 13). These effects will not be considered in this review.

The optical polarization $P(\mathbf{r}, t)$ is the only molecular quantity that appears in the Maxwell equations (54a,b). It serves as a source for the radiation field. Molecular motions and relaxation processes will therefore show up in optical measurements only through their effect on the polarization. Consequently, a complete knowledge of the optical polarization is sufficient for the interpretation of any spectroscopic measurement. The

calculation of the optical polarization is therefore the main goal of any theory of optical spectroscopy (47a–c, 55a,b). The optical polarization $P(\mathbf{r},t)$ is given by the expectation value of the dipole operator μ, $P(t) = \mathrm{Tr}[\mu\rho(t)]$, where $\rho(t)$ is the density matrix (56a–c), which satisfies the Liouville equation

$$\frac{d\rho}{dt} = -i[H,\rho] - i[H_{\mathrm{int}},\rho]. \qquad 2.$$

In this description $\rho(t)$ is viewed as a vector in *Liouville space* (in the same way that the wavefunction $\psi(t)$ is a vector in coordinate space) (47a–c, 55a,b). The time dependent density matrix allows the calculation of the expectation value of any molecular operator. It is common to expand the polarization in a power series in the electric field $E(\mathbf{r},t)$. The nth order term is denoted $P^{(n)}$. Each order in this expansion represents a different class of optical measurements (54a,b). The linear polarization $P^{(1)}$ is responsible for linear optics, $P^{(2)}$ represents second order nonlinear processes such as frequency sum generation (57a–c), and $P^{(3)}$ is the third order polarization, which represents a broad variety of four wave mixing techniques such as pump-probe spectroscopy. In this review I focus on optical techniques related to $P^{(3)}$. A straightforward expansion of the Liouville equation yields (47a–c)

$$P^{(1)}(\mathbf{r},t) = \int_0^\infty dt_1\, \hat{S}^{(1)}(t_1)E(\mathbf{r},t-t_1) \qquad 3a.$$

$$\hat{S}^{(1)}(t_1) = i[J(t_1) - J^*(t_1)] \qquad 3b.$$

$$J(t_1) = |\mu_{eg}|^2\langle \mathscr{G}_{eg}(t_1)\rho_g\rangle \qquad 3c.$$

Here $\langle\cdots\rangle$ denotes a quantum mechanical trace over the nuclear degrees of freedom and ρ_g is the initial equilibrium density matrix in the ground electronic state. The asterisk (*) represents the complex conjugate. We have introduced here the Green function $\mathscr{G}_{nm}(t)$ defined by its action on an ordinary nuclear operator A

$$\mathscr{G}_{nm}(t)A \equiv \exp(-iH_n t)A\exp(iH_m t), \qquad n,m = g,e,f. \qquad 4.$$

For clarity, we have invoked the Condon approximation, which assumes that the electronic transition dipole is independent of the nuclear coordinates. This approximation will be used in most of this review, unless otherwise stated. The nonlinear polarization $P^{(3)}$ is given by (47a–c, 58a–c)

$$P^{(3)}(\mathbf{r},t) = \int_0^\infty dt_1 \int_0^\infty dt_2 \int_0^\infty dt_3 \times \hat{S}^{(3)}(t_3,t_2,t_1)E(\mathbf{r},t-t_3)E(\mathbf{r},t-t_3-t_2)E(\mathbf{r},t-t_3-t_2-t_1). \qquad 5a.$$

$$\hat{S}^{(3)}(t_3,t_2,t_1) = i\sum_{i=1}^{4}[R_i(t_3,t_2,t_1) - R_i^*(t_3,t_2,t_1)] \qquad 5b.$$

$$R_1(t_3,t_2,t_1) = \sum_{v=f,g} |\mu_{ve}|^2|\mu_{eg}|^2\langle \mathscr{G}_{ve}(t_3)\mathscr{G}_{ee}(t_2)\mathscr{G}_{ge}(t_1)\rho_g\rangle$$

$$R_2(t_3,t_2,t_1) = \sum_{v=f,g} |\mu_{ve}|^2|\mu_{eg}|^2\langle \mathscr{G}_{ve}(t_3)\mathscr{G}_{ee}(t_2)\mathscr{G}_{eg}(t_1)\rho_g\rangle$$

$$R_3(t_3,t_2,t_1) = \sum_{v=f,g} |\mu_{ve}|^2|\mu_{eg}|^2\langle \mathscr{G}_{ve}(t_3)\mathscr{G}_{vg}(t_2)\mathscr{G}_{eg}(t_1)\rho_g\rangle$$

$$R_4(t_3,t_2,t_1) = \sum_{v=f,g} |\mu_{ve}|^2|\mu_{eg}|^2\langle \mathscr{G}_{vg}(t_3)\mathscr{G}_{vg}(t_2)\mathscr{G}_{ge}(t_1)\rho_g\rangle. \qquad 5c.$$

The linear response function $\hat{S}^{(1)}(t_1)$ and the nonlinear response function $\hat{S}^{(3)}(t_3,t_2,t_1)$ are the key quantities of the present formulation. They contain the complete microscopic information necessary for the calculation of any measurement related to $P^{(1)}$ and $P^{(3)}$, respectively. The eight terms in $\hat{S}^{(3)}$ ($R_1 \ldots R_4$ and their complex conjugates) correspond to eight distinct Liouville space pathways. In Figure 1 I display the Liouville space coupling scheme and the four pathways corresponding to $R_1 \ldots R_4$. Each pathway represents a different sequence of time evolutions of the density matrix, which undergoes three consecutive propagation periods. For R_1, for example, the system is in an optical coherence ρ_{ge} during the t_1 period. It then propagates in the excited state ρ_{ee} for the t_2 period and finally it is again in a coherence ρ_{ve} (with $v = g$ or f) for the t_3 period. The other R_i terms can be interpreted similarly. t_1, t_2, and t_3 are the time intervals between successive interactions with the radiation field.

The density matrix is widely used in the theory of linear optical lineshapes (47a–c, 56a–c), in magnetic resonance (59), and in the nonlinear optics of few-level systems (54a,b). For example, the Bloch equations describe the evolution of a two level system interacting with a strong radiation field and with a thermal bath. The effects of the bath are incorporated via phenomenological relaxation parameters representing level (T_1) relaxation and coherence (T_2) dephasing. These equations cannot be directly applied to the spectroscopy of complex molecular systems, such as solvated dyes, which require a more microscopic treatment. In the present approach I have used the density matrix to formulate the problem with multitime correlation functions (47a–c, 50, 55a,b, 58a–c). Correlation functions provide a natural link between theory and experiment. They are

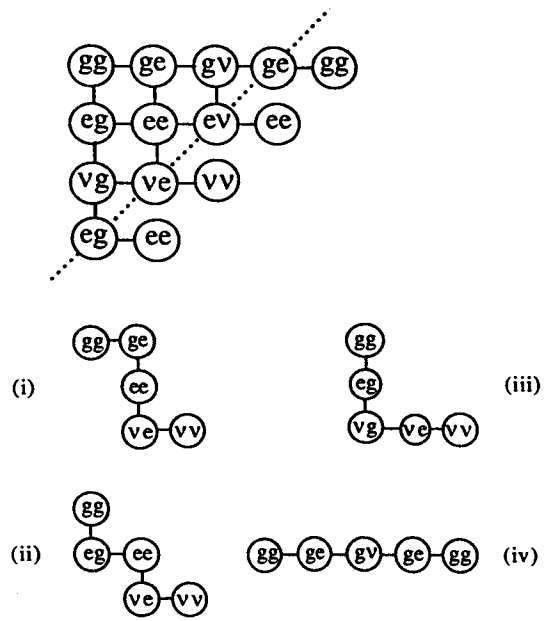

Figure 1 The Liouville space coupling scheme and the four pathways contributing to the nonlinear response function (48). Initially the electronic density matrix is $|g\rangle\langle g|$, which is denoted *gg* in the *upper left corner*. *Solid lines* denote the dipole interaction μ. A *horizontal* (*vertical*) line represents an action of μ from the *right* (*left*). Starting at the *upper left corner* there are $2^3 = 8$ third order pathways in Liouville space, which lead to the *dashed line* and contribute to the third order density matrix $\rho^{(3)}$. *v* stands for either *g* or *f* (see Eq. 5b). Out of the eight pathways, (i) (ii), (iii), and (iv) are shown in the Figure and they correspond to R_1, R_2, R_3, and R_4, respectively, of Eq. 5b. The other four pathways are the complex conjugates of these pathways.

defined without alluding to a particular technique; consequently, they unify a large body of information and clarify the interrelationships among the various techniques. The linear and the nonlinear response functions may be also expressed in terms of amplitudes and wavefunctions rather than in terms of the density matrix (47, 58). This form is useful in the absence of a thermal bath or when the bath has a very different timescale than the system. In this case the detailed dynamics of the bath is not relevant, and its effect can be simply modeled as purely homogeneous or inhomogeneous line broadening (see Eqs. 21 and 22). Many calculations have used this simplified picture (17b,c), which is a special case of the present formulation. In the coming sections I shall specialize to a few of the most common ultrafast techniques and discuss them in detail.

THE DOORWAY/WINDOW PICTURE OF PUMP-PROBE SPECTROSCOPY

In a pump-probe experiment the system is subjected to two light pulses: the pump pulse with wavevector $\mathbf{k}_1$ whose frequency is centered around ω_1, and the probe pulse with wavevector $\mathbf{k}_2$ whose frequency is centered around ω_2. We assume that the pump frequency ω_1 is tuned near resonance with ω_{eg} and it can only induce a $|g\rangle$ to $|e\rangle$ transition, whereas the probe frequency ω_2 is tuned near resonance with ω_{fe} and can only induce an $|e\rangle$ to $|f\rangle$ transition. The time delay τ of the probe pulse with respect to the pump pulse is continuously varied.

We shall consider the probe differential absorption, defined as the total probe absorption in the presence of pump minus the probe absorption in the absence of the pump. To lowest order in the pump and the probe intensities, the differential absorption is given by (48)

$$S(\omega_1, \omega_2; \tau) = 2\omega_2 \operatorname{Im} \int_{-\infty}^{\infty} dt\, E_2^*(t) P^{(3)}(\mathbf{k}_2, t) \qquad 6.$$

where $E_2(t)$ is the probe envelope and $P^{(3)}(\mathbf{k}_2, t)$ is the $\mathbf{k}_2$ spatial Fourier component of $P^{(3)}$. The number of terms contributing to Eq. 6 together with Eq. 5a, when the incoming pulses are decomposed into Fourier components, is very large. Fortunately only six of them survive if we make the rotating wave approximation (RWA), i.e. consider only resonant processes in which the laser frequencies appear in the form $\omega_1 - \omega_{eg}$ and $\omega_2 - \omega_{fe}$ and neglect off resonant $\omega_1 + \omega_{eg}$ and $\omega_2 + \omega_{ef}$ terms. Double-sided Feynman diagrams (60a,b) provide a useful bookkeeping device for the various terms and interactions in the calculation of the molecular polarization. The rules for these diagrams are as follows: (*a*) the density matrix is represented by two vertical lines (the line on the left represents the ket and the line on the right represents the bra); (*b*) the time runs vertically from bottom to top; (*c*) an interaction with the radiation field is represented by a wavy line; (*d*) each interaction is assigned an arrow and labeled by the corresponding field, ω_j. Incoming arrows represent photon absorption while outgoing arrows represent photon emission. Only six diagrams are relevant for pump-probe spectroscopy (48), the three shown in Figure 2 and their complex conjugates. The representation of Figure 1 shows only the molecular density matrix. The Feynmann diagrams in Figure 2 show also the time ordering of the fields and the choice of frequencies. In the remainder of this section I first introduce three conditions that the laser pulses may satisfy (49). I then show that the "snapshot" picture is recovered when all three conditions are simultaneously met. Extensions of this picture to more general cases are discussed as well.

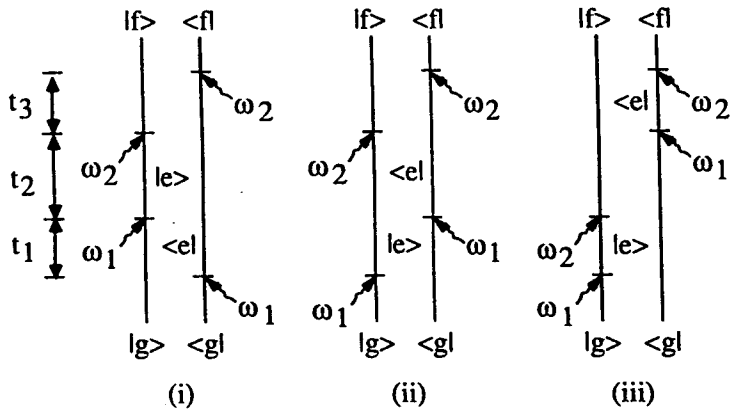

Figure 2 The three double-sided Feynman diagrams representing the probe difference absorption in the RWA. Time runs from the bottom to the top. t_1, t_2, and t_3 are the intervals between successive interactions.

Well-Separated Pulses (WSP)

The general expression for the probe absorption is considerbly simplified when the pump pulse and the probe pulse are well separated in time (i.e. their delay τ is much longer than their durations). The two terms, represented by diagrams (*i*) and (*ii*) of Figure 2, describe processes in which the system interacts first with the pump and then with the probe field. The term (*iii*) of Figure 2, describes processes in which one of the interactions with the probe field E_2 takes place between two interactions with the pump. If the delay time τ between the pump and the probe is large compared with their temporal width, we can enforce the time ordering of "pump first and probe second." In this case the contribution of (*iii*) will be negligible compared with (*i*) and (*ii*). In addition, (*i*) and (*ii*) will be simplified.

Pulses Short Compared with Nuclear Dynamics (PSN)

Naturally if we wish to probe a certain dynamical process (a molecular vibration, bond breaking, curve crossing) we need laser pulses of comparable or shorter duration in order to have the proper temporal resolution. The PSN condition implies that the pulses are much shorter than the nuclear dynamics being probed; we can then neglect the nuclear motions during the pulses.

Pulses Long Compared with Electronic Dephasing Timescale (PLD)

When the time integrations in Eqs. 5a are carried out, we find that t_1 is the time it takes for the ω_1 photon to be absorbed. During the t_1 interval

the system is in an electronic (optical) coherence given by the off diagonal density matrix element ρ_{eg} or ρ_{ge} (Figure 2). Its evolution is determined by a quantum mechanical phase resulting from the difference between H_g and H_e. When this phase is averaged over the ensemble of initial conditions for nuclear motions, it causes a decay denoted *electronic dephasing*. This electronic dephasing, which controls the duration of the t_1 interval, has contributions from both Franck-Condon active molecular vibrations and low frequency intramolecular or solvent modes. Electronic dephasing is also responsible for the broadening of the linear absorption line from g to e. A good estimate for the dephasing timescale is given by the inverse absorption linewidth for the g to e transition. Similar arguments apply to t_3, which is the time interval it takes the ω_2 probe photon to be absorbed. t_3 is restricted by the timescale of electronic dephasing between the e and f states (i.e. the inverse linewidth of the e to f absorption). Femtosecond experiments are normally conducted on systems with broad spectral lines where individual eigenstates are not resolved. This implies very fast dephasing. The PLD condition states that the laser pulses are much longer than this ultrafast dephasing timescale. We can then assume that the pulse envelopes do not vary during the t_1 and t_3 intervals.

Now I shall discuss various limiting cases in which all or some of the above conditions hold (48, 49).

CASE I The first case occurs when all three conditions (WSP, PSN, and PLD) hold simultaneously. We can then recast Eqs. 6 and 5a in the form:

$$S_0(\omega_1,\omega_2;\tau) = \langle \rho_W(\omega_2)\mathcal{G}_{ee}(\tau)\rho_D(\omega_1)\rangle \equiv Tr[\rho_W(\omega_2)\exp(-iH_e\tau)\rho_D(\omega_1)\exp(iH_e\tau)] \quad 7.$$

where we have defined the *doorway state*

$$\rho_D(\omega_1) \equiv \int_0^\infty dt_1 \exp(i\omega_1 t_1)[\exp(-iH_e t_1)\mu_{eg}\rho_g \exp(iH_g t_1)\mu_{ge}] + \text{h.c.} \quad 8a.$$

and the *window state*

$$\rho_W(\omega_2) \equiv \int_0^\infty dt_3 \exp(i\omega_2 t_3)[\exp(iH_e t_3)\mu_{ef}\exp(-iH_f t_3)\mu_{fe}] + \text{h.c.} \quad 8b.$$

In Eq. 7, field strength factors have been dropped and h.c. denotes the hermitian conjugate. S_0 will be denoted the *snapshot spectrum* (48) (in Ref. 48 the "snapshot" spectrum was denoted the "bare" spectrum). This spectrum does not depend on the light pulse shapes but only on their frequencies ω_1 and ω_2; it is an intrinsic molecular property (although proper light pulses are essential in order to observe the snapshot spectrum).

Note that the doorway and the window states represent a molecular density matrix. Also, in these definitions we did not invoke the Condon approximation; that is, we kept the nuclear dependence of the electronic dipole. The corresponding vibronic eigenstates of H_g, H_e, and H_f will be denoted as $|\alpha\rangle$, $|\beta\rangle$, $|\gamma\rangle$ with eigenvalues ε_α, ε_β and ε_γ, respectively. When Eqs. 8 are expanded by using the molecular vibronic eigenstates, we get

$$\rho_D(\beta\beta';\omega_1) \equiv \langle\beta|\rho_D(\omega_1)|\beta'\rangle$$

$$= i\sum_\alpha P(\alpha)\mu_{\beta\alpha}\mu_{\alpha\beta'}\left[\frac{1}{\omega_1-\omega_{\beta\alpha}+i\Gamma_{\beta\alpha}}-\frac{1}{\omega_1-\omega_{\beta'\alpha}-i\Gamma_{\beta'\alpha}}\right] \quad 9a.$$

and

$$\rho_W(\beta'\beta;\omega_2) \equiv \langle\beta'|\rho_W(\omega_2)|\beta\rangle$$

$$= i\sum_\gamma \mu_{\beta'\gamma}\mu_{\gamma\beta}\left[\frac{1}{\omega_2-\omega_{\gamma\beta'}+i\Gamma_{\gamma\beta'}}-\frac{1}{\omega_2-\omega_{\gamma\beta}-i\Gamma_{\gamma\beta}}\right]. \quad 9b.$$

In Eqs. 9 the doorway and the window functions are expanded in the $|\beta\rangle$ representation and $\rho_D(\beta\beta';\omega_1)$ and $\rho_W(\beta'\beta;\omega_2)$ are their $\beta\beta'$ matrix elements, respectively. $\omega_{vv'} \equiv \varepsilon_v - \varepsilon_{v'}$ and $\Gamma_{vv'}$ is a phenomenological damping rate. The probe absorption is then given by

$$S_0(\omega_1,\omega_2;\tau) = \sum_{\beta\beta'}\rho_W(\beta'\beta;\omega_2)\exp(-i\omega_{\beta\beta'}\tau-\Gamma_{\beta\beta'}\tau)\rho_D(\beta\beta';\omega_1). \quad 10.$$

Equations 7 or 10 offer the following physical picture of the pump probe experiment. The pump field transfers a fraction of the molecules from the ground state to the excited state, $\rho_D(\omega_1)$ representing the density matrix of the excited molecules. Similarly, the probe field creates the window state $\rho_W(\omega_2)$. Equations 7 or 10 imply that the probe absorption can be calculated by taking the doorway state, propagating it for the delay period on the excited potential surface [as given by $\mathcal{G}_{ee}(\tau)$], and then calculating its overlap with the window state. For $\beta = \beta'$, $\rho_D(\beta\beta';\omega_1)$ is the *population* of level β in that wavepacket. For $\beta \neq \beta'$ this is the *coherence* between the two states. The denominator $\omega_1-\omega_{\beta\alpha}$ selects preferentially states β that are near resonance $\omega_1 = \omega_{\beta\alpha}$. Note also that creating a coherence requires both states β and β' to be coupled to the same vibronic state α. $\rho_W(\beta'\beta;\omega_2)$ is a wavepacket that the probe selects. It reflects the contribution of the coherence between β and β' to the absorption of a ω_2 photon.

The classical interpretation is even more apparent if we express the doorway and the window states in the *Wigner representation* (61). In this representation the density matrix is a function of the coordinates $\mathbf{q}$ and momentum $\mathbf{p}$, i.e. a function in phase space. This is an exact quantum

representation, which in the classical limit reduces naturally to the classical density matrix. We denote the Wigner representation of $\rho_D(\omega_1)$ and $\rho_W(\omega_2)$ by $\rho_D(\mathbf{pq};\omega_1)$ and $\rho_W(\mathbf{pq};\omega_2)$. Eq. 10 thus assumes the appealing form

$$S_0(\omega_1,\omega_2;\tau) = \iiiint d\mathbf{p}\,d\mathbf{q}\,d\mathbf{p}'\,d\mathbf{q}'\,\rho_W(\mathbf{pq};\omega_2)\mathcal{G}_{ee}(\mathbf{pq}\tau;\mathbf{p}'\mathbf{q}')\rho_D(\mathbf{p}'\mathbf{q}';\omega_1). \quad 11.$$

ρ_D is now the density matrix (in phase space) prepared by the pump. ρ_W is the corresponding window and $\mathcal{G}_{ee}(\mathbf{pq}\tau;\mathbf{p}'\mathbf{q}')$ is the quantum mechanical propagator from phase space point $\mathbf{p}'\mathbf{q}'$ to $\mathbf{pq}$ at time τ. Equations 10 and 11 are identical but in different representations. When the relevant vibronic levels are sparse, the state representation may be adequate and the signal may show quantum beats (4–9a,b). When the states are very dense (e.g. ICN photodissociation) (25a–c), the phase space description is more useful.

CASE II In this case we invoke the WSP and PSN conditions. When the pulses are short compared with the molecular nuclear dynamics but not necessarily long compared with the dephasing we get

$$S(\omega_1,\omega_2;\tau) = \iint d\omega_1'\,d\omega_2'\,I_1(\omega_1-\omega_1')I_2(\omega_2-\omega_2')S_0(\omega_1',\omega_2';\tau) \quad 12a.$$

where I_1 and I_2 are the power spectra of the pump and the probe pulses, respectively, i.e.

$$I_j(\omega) = \frac{1}{2\pi}\left|\int_{-\infty}^{\infty} dt\,E_j(t)\exp(-i\omega t)\right|^2. \quad 12b.$$

Since the pulses are short, their power spectrum may be broad, and the actual spectrum is given by a *spectral convolution* of the snapshot spectrum S_0 with the pulse intensity profiles.

CASE III We now invoke the WSP and the PLD conditions. When the pulses are long compared with the electronic dephasing timescale but not necessarily short compared with the nuclear dynamics we get

$$S(\omega_1,\omega_2;\tau) = \int_0^\infty dt\,I(\tau-t)S_0(\omega_1,\omega_2;t) \quad 13a.$$

with $I(t)$ being the temporal profile

$$I(t) = \int d\tau'\,|E_1(\tau')|^2|E_2(t-\tau')|^2. \quad 13b.$$

Since the pulses are long, the time resolution may be compromised and the actual spectrum is given by a *temporal convolution* of the snapshot spectrum with the pulse intensity profiles.

CASE IV In this case we start with Case I where we assume the WSP, PSN, and the PLD conditions to hold. In addition we shall consider the classical limit, where we assume that the optical transition occurs instantaneously, and further, the transition dipole does not depend on the nuclear coordinates (the Condon approximation). Assuming that the various operators in Eqs. 8 commute we obtain

$$S_0(\omega_1,\omega_2;\tau) = 4\pi^2|\mu_{cg}|^4\langle\delta(\omega_2-U_{fc})\mathcal{G}_{cc}(\tau)\delta(\omega_1-U_{eg})\rho_g\rangle \qquad 14.$$

where $U_{eg} \equiv H_e - H_g$ and $U_{fe} \equiv H_f - H_e$. This result has a simple classical interpretation, related to the *classical Condon approximation* (62a,b), which states that a photon ω can be absorbed or emitted only in nuclear configurations with $U = \omega$. The initial doorway state is $\sim\delta(\omega_1 - U_{eg})\rho_g$. Its subsequent evolution for the delay period τ is governed by the excited state Hamiltonian H_e. The probe pulse creates a window function $\delta(\omega_2 - U_{fc})$. The spectrum is given by the overlap of the propagated doorway state with the window state.

CASE V When only the WSP condition holds, the doorway/window picture and Eq. 7 are still valid, but the definition of the doorway and the window states becomes more complicated. In this case they depend on the field amplitudes and phases and not only on the field intensities (49).

CASE VI Cases I–V were all based on the RWA and additional assumptions. If we just invoke the RWA, the signal is still given by Eqs. 6 and 5a with the three terms shown in Figure 2. The third term gives rise to a spike at short delay times known as the coherent artifact (58b, 63a,b). In this case the doorway/window picture does not hold and we need to treat the spectrum as a single four wave mixing event, calculate $\hat{S}^{(3)}$, and then perform the triple time integration. This procedure is complicated because a complete knowledge of $\hat{S}^{(3)}$ for all values of t_1, t_2, and t_3 allows the calculation of the spectrum for all ω_1, ω_2, τ, and for arbitrary field profiles $E_1(t)$ and $E_2(t)$. The doorway/window picture allows a much simpler calculation with a more modest goal; the probe absorption signal is calculated for a given pump frequency ω_1, probe frequency ω_2, and a limited range of delay times τ. This picture no longer holds in Case VI.

CASE VII If we do not invoke the RWA, the picture becomes more complicated. The number of relevant terms is no longer the three terms shown in Figure 2 but much larger. If ω_{eg} and ω_{fe} are not well separated and we allow both fields to interact with both transitions, the number of terms becomes even larger.

We have used the model system shown in Figure 3 to calculate the probe absorption in the ICN photodissociation (64). The time resolved probe absorption is shown in Figure 4 for the three values of ω_2 marked in Figure 3. We find that for ω_2 values selecting short delay times (*upper panel*), the signal can be adequately calculated by using the classical Condon approximation for the snapshot spectrum followed by a temporal convolution with the pulses (Eqs. 14 and 13). For ω_2 values selecting long delay times (*lower panel*), a spectral convolution is appropriate (Eqs. 14 and 12). The reason is that the probe absorption lineshape is initially broad and it gradually narrows as the bond dissociates. For large internuclear separations, the spectrum is infinitely narrow. Consequently at short times the pulses are long compared with the electronic dephasing, whereas for long times the pulses are short compared with the electronic dephasing. The analysis of Bernstein & Zewail (26b), which is essentially equivalent to Eqs. 14 and 12, seems therefore to apply reasonably well for long delay times but breaks down for shorter delays.

When analyzing pump-probe spectroscopy we note an apparent con-

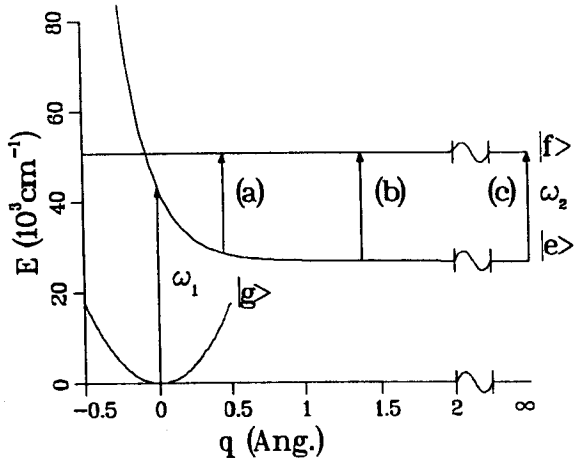

Figure 3 Potential surfaces for the model system for ICN pump-probe spectroscopy. q represents the I–C separation with $q = 0$ being the ground state bond length. The three transitions marked (a), (b), and (c) are for different probe detunings, $\omega_2 - \omega_{fe} = -2400$, -590 and 0 cm^{-1}, respectively. ω_{fe} is the electronic transition energy at infinite internuclear separation. The classical Condon transition for these detunings ($U_{fe}(q_c) = \omega_2$) is at $q_c = 0.5$ Å, 1.4 Å, and ∞, respectively.

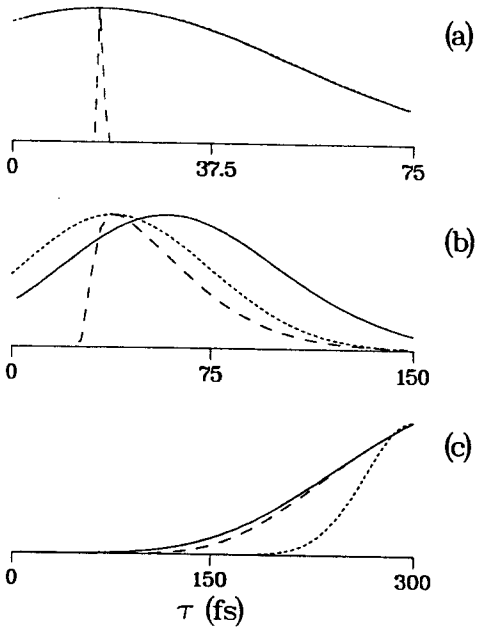

Figure 4 The probe absorption is plotted versus the delay time for the three values of the probe detuning $\omega_2-\omega_{fe}$ shown in Figure 3. The pump is tuned on resonance (Figure 3); 50 fsec pump and probe pulses were used in this calculation (64).

Solid line—exact calculation obtained by numerically solving the Schrödinger equation. *Long dashed line*—calculation using the classical Condon approximation and Case II (Eqs. 12 and 14). *Short dashed line*—calculation using the classical Condon approximation and Case III (Eqs. 13 and 14).

tradiction. The temporal resolution (τ) and the spectral resolution of ω_2 are controlled by different instruments. For example, the experiment can be performed by using an infinitely short probe and then dispersing it spectrally with infinite resolution (8a,b). In this case, Eq. 8b for the window function is exact (49). This seems to imply that we know the frequency of the ω_2 photon and the time in which it was absorbed with infinite accuracy, in violation of the Heisenberg uncertainty relation! This argument is, however, incorrect. Although τ may be fixed accurately, the actual time between the pump and the probe absorption events has an uncertainty resulting from the finite time it takes for the pump and the probe photons to be absorbed (t_1 and t_3, respectively). If the pulses are short and if the lineshapes are broad so that $t_1, t_3 \ll \tau$ (fast dephasing), then the actual delay time is τ and the temporal resolution is high. However, since the

lineshapes are broad, we do not know ω_2 to a better accuracy than the linewidth. Conversely, if the lines are narrow we lose the temporal resolution (since t_1 and t_3 are long) but we get good spectral resolution. No useful information is obtained when femtosecond experiments are performed on narrow spectral lines; the genuine temporal resolution of the experiment is determined by the pulses as well as by the system being probed (65a). One cannot necessarily assume that if the pulses are short and their delay τ is determined with infinite accuracy, then the actual delay between the pump and the probe absorption events is τ. Quantum mechanical principles will determine the actual delay, and only when the spectral lines are broad will it be equal to τ.

MULTIMODE BROWNIAN OSCILLATOR MODEL FOR POLYATOMIC MOLECULES

Many of the current experiments on solvated dyes (3–9) can be interpreted by using a two level model. The two level model is a special case of Eqs. 1 and 5b whereby we eliminate the level f and set $v = g$. We assume that the nuclear motions can be decomposed into harmonic modes (49, 50, 65a–c). The frequency and the dimensionless coordinate of the jth mode are denoted Ω_j and q_j, respectively. The equilibrium position of q_j is $q_j = 0$ for the ground state and $q_j = -d_j$ for the excited state, d_j is the dimensionless equilibrium displacement of this mode in the two electronic states. We further assume that each mode undergoes Brownian motion with a friction function γ_j (66a,b) and set $\mu_{eg} = 1$. The linear response function for this model is given by Eq. 3b with

$$J(t) = \exp[-i\omega_{eg}t - g(t)]. \tag{15.}$$

$g(t)$ is the line broadening function

$$g(t) = \sum_j \left[i\lambda_j \int_0^t dt' M_j(t') + \Delta_j^2 \int_0^t dt' \int_0^{t'} dt'' M_j(t'') \right], \tag{16.}$$

where $\lambda_j \equiv \frac{1}{2}d_j^2\Omega_j$, $\Delta_j^2 \equiv (\bar{n}_j+\frac{1}{2})d_j^2\Omega_j^2$, and $\bar{n}_j \equiv [\exp(\hbar\Omega_j/k_BT)-1]^{-1}$. $\bar{n}_j$ denotes the thermal occupation number of the jth mode, with k_B being the Boltzman constant and T the temperature. In the high temperature limit $k_BT \gg \hbar\Omega_j$ we have $\Delta_j^2 \cong 2\lambda_j k_BT$. $M_j(t)$ is the normalized ground state correlation function of the oscillator, which satisfies the equation

$$\ddot{M}_j(t) + \gamma_j\dot{M}_j(t) + \Omega_j^2 M_j(t) = 0, \tag{17.}$$

with $M_j(0) = 1$ and $\dot{M}_j(0) = 0$. The linear absorption lineshape, in the present model, is given by (47a–c)

$$\sigma_A(\omega) = \frac{1}{\pi}\mathrm{Re}\int_0^\infty dt \exp[i(\omega-\omega_{eg})t]\exp[-g(t)]. \quad 18.$$

The fluorescence lineshape σ_F for this model is the mirror image of σ_A, i.e. $\sigma_F(-\omega) = \sigma_A(\omega)$. The nonlinear response function is given by Eq. 5 with (50, 58a–c)

$$R_1(t_3,t_2,t_1) = \exp(i\omega_{eg}t_1 + i\omega_{eg}t_3)\exp[-g(t_3)-g^*(t_1)-f_+^*(t_3,t_2,t_1)] \quad 19a.$$

$$R_2(t_3,t_2,t_1) = \exp(-i\omega_{eg}t_1 + i\omega_{eg}t_3)\exp[-g(t_3)-g(t_1)+f_+(t_3,t_2,t_1)] \quad 19b.$$

$$R_3(t_3,t_2,t_1) = \exp(-i\omega_{eg}t_1 + i\omega_{eg}t_3)\exp[-g^*(t_3)-g(t_1)+f_-(t_3,t_2,t_1)] \quad 19c.$$

$$R_4(t_3,t_2,t_1) = \exp(i\omega_{eg}t_1 + i\omega_{eg}t_3)\exp[-g^*(t_3)-g^*(t_1)-f_-^*(t_3,t_2,t_1)], \quad 19d.$$

where

$$f_-(t_3,t_2,t_1) = g(t_2)-g(t_2+t_3)-g(t_1+t_2)+g(t_1+t_2+t_3) \quad 19e.$$

$$f_+(t_3,t_2,t_1) = g^*(t_2)-g^*(t_2+t_3)-g(t_1+t_2)+g(t_1+t_2+t_3). \quad 19f.$$

Both the linear and the nonlinear response functions for this model can be expressed in terms of the lineshape function $g(t)$. This function depends in turn on two static parameters λ_j, Δ_j, and the normalized and real correlation function $M_j(t)$. Δ_j^2 is the variance of the nuclear displacement q_j and λ_j represents its coupling strength to the electronic transition.

The Brownian oscillator model can represent high frequency intramolecular vibrations as well as the low frequency local librations or local or collective solvent motions. These behaviors are apparent when the explicit form of the oscillator correlation function, obtained by solving Eq. 17, is considered.

$$M_j(t) = \begin{cases} \exp(-\gamma_j t/2)\left(\cos\bar{\omega}_j t + \dfrac{\gamma_j}{2\bar{\omega}_j}\sin\bar{\omega}_j t\right) & \gamma_j < 2\Omega_j \\ \exp(-\gamma_j t/2)(1+\gamma_j t/2) & \gamma_j = 2\Omega_j \\ \dfrac{s_+}{s_+-s_-}\exp(-s_- t) - \dfrac{s_-}{s_+-s_-}\exp(-s_+ t) & \gamma_j > 2\Omega_j \end{cases} \quad 20.$$

Here $\bar{\omega} \equiv [\Omega_j^2-(\gamma_j/2)^2]^{1/2}$, $s_\pm \equiv \gamma_j/2 \pm [(\gamma_j/2)^2-\Omega_j^2]^{1/2}$. When $\gamma_j = 0$, the oscillator experiences a coherent motion with $M_j(\tau) = \cos\Omega_j\tau$. For the high frequency modes with a finite but small damping ($\gamma_j < 2\Omega_j$) the oscillator motion is underdamped. When $\gamma_j > 2\Omega_j$ the motion becomes overdamped

and loses its coherent oscillatory motion. For the borderline case $\gamma_j = 2\Omega_j$ the oscillator is critically damped. The strongly overdamped case $\gamma_j \gg 2\Omega_j$ is of particular interest. In this limit, which applies to low frequency vibrations, we have $M_j(t) = \exp(-\Lambda_j t)$ with $\Lambda_j = \Omega_j^2/\gamma_j$. The oscillator motion in this case can be described by a Smoluchowski equation, since the momentum equilibrates rapidly (50, 66a,b). If we further set $\lambda_j = 0$, this model reduces to the stochastic model of spectral lineshapes (67–68a,b). Depending on the relative magnitude of Δ_j and the inverse timescale Λ_j, it can represent different cases, which are outlined below.

INHOMOGENEOUS BROADENING When $\Lambda_j = 0$ the nuclear configurations are static. We then have $g(t) = i\lambda_j t + \frac{1}{2}\Delta_j^2 t^2$. The absorption (Eq. 18) and the fluorescence lineshapes in this case are Gaussian with a width Δ_j and centered around $\omega_{eg}+\lambda_j$ and $\omega_{eg}-\lambda_j$, respectively. The Stokes shift, i.e. the difference between the absorption and the fluorescence peaks, is equal to $2\lambda_j$. We further get (68a,b)

$$R_1(t_3,t_2,t_1) = R_4(t_3,t_2,t_1) = \exp[i\lambda_j(t_1+t_3)-\tfrac{1}{2}\Delta_j^2(t_1+t_3)^2] \quad 21a.$$

$$R_2(t_3,t_2,t_1) = R_3(t_3,t_2,t_1) = \exp[i\lambda_j(t_3-t_1)-\tfrac{1}{2}\Delta_j^2(t_3-t_1)^2]. \quad 21b.$$

When the nuclei are not static but have slow motions ($\Lambda_j \ll \Delta_j$), the system will show spectral diffusion (69a,b). Time dependent Stokes shift measurements in solution (65a–c, 70–71) are usually interpreted in this limit.

HOMOGENEOUS BROADENING This is the extreme case opposite to inhomogeneous broadening. In the homogeneous broadening limit, the solvent nuclear relaxation is infinitely fast $\Lambda_j \gg \Delta_j$, i.e. $M_j(t) = \Lambda_j^{-1}\delta(t)$, and we have $g_j(t) = i(\lambda_j/\Lambda_j)t + \hat{\Gamma}_j t$, with $\hat{\Gamma}_j \equiv \Delta_j^2/\Lambda_j$. When $\lambda_j \ll \Lambda_j$, the absorption and the fluorescence lineshapes assume a Lorentzian form centered around ω_{eg} with the width equal to the dephasing rate $\hat{\Gamma}_j$. The Stokes shift vanishes in this case due to the rapid nuclear motions. The nonlinear response functions are given by (68a,b)

$$R_\alpha(t_3,t_2,t_1) = \exp[-\hat{\Gamma}(t_1+t_3)] \qquad \alpha = 1,\ldots,4. \quad 22.$$

In summary, the strongly overdamped Brownian oscillator model provides a simple and exactly solvable model that interpolates continuously between the inhomogeneous and the homogeneous limits as Λ_j/Δ_j is increased.

ULTRAFAST RESONANT SPECTROSCOPIES: PUMP-PROBE, HOLE-BURNING, AND PHOTON ECHOES

When the light pulses are very short, the theoretical description simplifies considerably. Various time integrations in the definitions of the doorway

and the window functions and in the optical signal can be eliminated and a semiclassical picture becomes more appropriate. In this section I review some of the most common impulsive resonant techniques that use the two-level multimode Brownian oscillator model.

Impulsive Resonant Pump-Probe Spectroscopy

When the probe absorption is calculated using Eq. 6 for the two level model, we find that the expression has more terms than for the three level model. The reason is that now both fields interact with the same optical transition. The snapshot spectrum (Case I) thus becomes (49, 65a–c)

$$S_0(\omega_1,\omega_2;\tau) \equiv \langle \rho_W(\omega_2)\mathcal{G}_{ee}(\tau)\rho_D(\omega_1)\rangle + \langle \bar{\rho}_W(\omega_2)\mathcal{G}_{gg}(\tau)\bar{\rho}_D(\omega_1)\rangle. \quad 23.$$

The first term is identical to Eq. 7 with the final state f replaced by g. The second term is a new term with a new doorway and window function: $\bar{\rho}_D$ and $\bar{\rho}_W$. Equation 23 provides the following physical picture of the pump probe experiment. The pump field transfers a fraction of the molecules from the ground state to the excited state, creating a "particle" in the excited electronic state, and a "hole" in the ground electronic state. The first term in Eq. 23 represents the particle contribution. The second term represents the hole, which has its own doorway and window and propagates on the ground state potential surface (Figure 5). Exact expressions

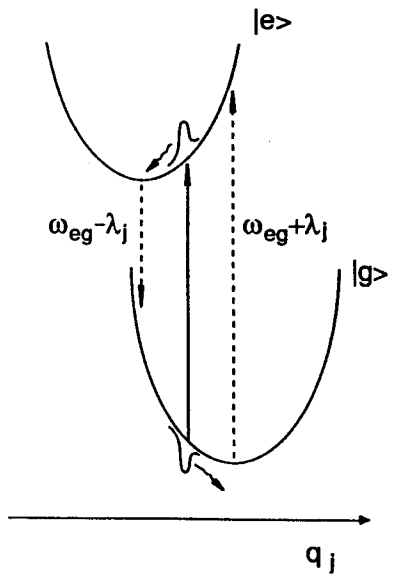

Figure 5 Pump-probe measurement and the dynamical Stokes shift for a strongly overdamped mode in the spectral diffusion limit. The potential function for the nuclear mode has a displaced equilibrium position in the ground and in the excited electronic states. Shown is the excited state "particle" and the ground state "hole" relaxation. For the excitation wavelength shown (*solid arrow*), the particle and the hole contributions to the absorption undergo a time dependent red and a blue shift, respectively. The stationary absorption and the fluorescence maxima are at $\omega_{eg}+\lambda_j$ and $\omega_{eg}-\lambda_j$, respectively.

for the doorway and the window functions for the Brownian oscillator model have been derived (49). The time and frequency resolved fluorescence in this case is given by the first term in Eq. 23, i.e. the particle contribution (9a,b, 47b, 65a–c).

We next consider the probe absorption when the pump pulse is infinitely short (impulsive). The probe field is short compared with the molecular nuclear dynamics but is long compared with the dephasing timescale. In this case, we can use Eq. 12 with $I_1(\omega_1)$ broad and flat and $I_2(\omega_2)$ very narrow. We then get

$$S(\omega_2;\tau) = 2\mathrm{Re}\int_0^\infty dt_3 \exp(-i\omega_2 t_3) \times [\langle \mathcal{G}_{ge}(t_3)\mathcal{G}_{ee}(\tau)\rho_g\rangle + \langle \mathcal{G}_{ge}(t_3)\mathcal{G}_{gg}(\tau)\rho_g\rangle]. \quad 24.$$

Here the first and second terms are related to R_2 and R_3 and represent the particle and the hole contributions, respectively. Their calculation requires propagating the molecular system in the electronic coherence $|g\rangle\langle e|$ during the t_3 period, as well as in electronic population $|e\rangle\langle e|$ or $|g\rangle\langle g|$ during the delay time τ period. Note that within the Condon approximation the hole contribution does not depend on the time delay τ since $\mathcal{G}_{gg}(\tau)\rho_g = \rho_g$. A final closed expression for the impulsive absorption of the multimode Brownian oscillator model can be obtained by substituting Eqs. 19 in Eq. 24. At short delay times τ, the particle and the hole contributions to the probe absorption are identical. For long delay times the signal splits into two components with reflection symmetry, i.e. the hole contribution at $\omega_2-\omega_{eg}$ equals the particle contribution at $-(\omega_2-\omega_{eg})$. This behavior is illustrated in Figure 6 (72).

Hole-Burning Spectroscopy

The electronic transition frequency ω_{eg} for molecules in condensed phases has a static distribution due to changes in local environment. This results in a contribution to $J(t)$ that enters as a convolution of the linear absorption lineshape with a broad envelope (hundreds of wavenumbers). The useful dynamical information of $J(t)$ is often "buried" under this envelope, which is denoted inhomogeneous broadening (73). As a result, absorption lineshapes usually carry very little dynamical information. This state of affairs is typical for spectra in solution, liquids, glasses, polymers, proteins, and molecular crystals. In many cases, inhomogeneous broadening results from a large number of small contributions from various molecules in the sample. The central limit theorem then implies that the spectrum should have a Gaussian profile (56a–c, 67a–c, 69a,b). A good example is the overdamped Brownian oscillator in the static limit. It should be empha-

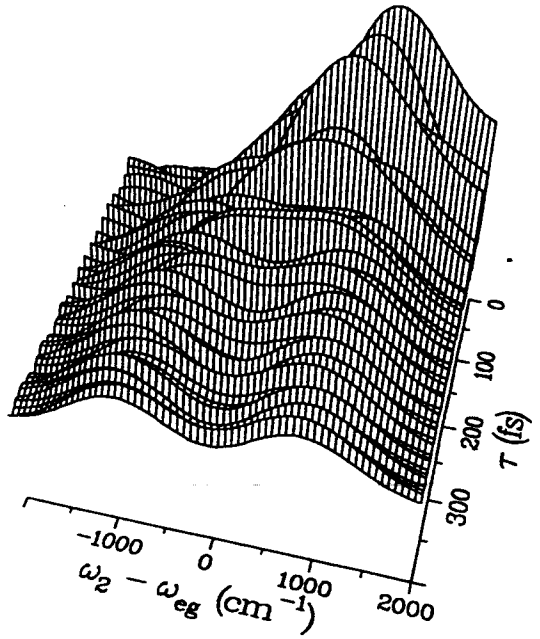

Figure 6 (*a*) The time and frequency resolved differential absorption spectrum for the multimode Brownian oscillator model (Eq. 24) (72). The model has two coherent modes $\omega_1 = 600\ \text{cm}^{-1}$, $d_1 = 1.2$, $\omega_2 = 1800\ \text{cm}^{-1}$, $d_2 = 1$, $\gamma_1 = \gamma_2 = 60\ \text{cm}^{-1}$, and one overdamped mode with $\Delta_3 = 520\ \text{cm}^{-1}$, $\Lambda_3 = 52\ \text{cm}^{-1}$, $T = 300\text{K}$.

sized, however, that inhomogeneous line profiles are not necessarily Gaussian, and other forms appear in various situations (73). When the nuclei are static, the response function can be calculated exactly for an arbitrary distribution (not necessarily Gaussian). It follows from Eqs. 5 that the inhomogeneous contribution to R_1 and R_4 is $\chi(t_1+t_3)$ and the contribution to R_2 and R_3 is $\chi(t_3-t_1)$ where $\chi(t)$ is the Fourier transform of the inhomogeneously broadened lineshape. Equations 21 are a special case when $\chi(t)$ is Gaussian.

Nonlinear optical techniques such as hole-burning and photon echo spectroscopies are capable of eliminating the effects of inhomogeneous broadening, and providing valuable dynamical information even when linear optical measurements are broad and structureless (36a–c, 52, 72). I shall consider the hole-burning first and then discuss photon echoes. The hole-burning technique is the same as the pump-probe but is used when the system has large inhomogeneous broadening, much larger than the other electronic dephasing. We then get (72)

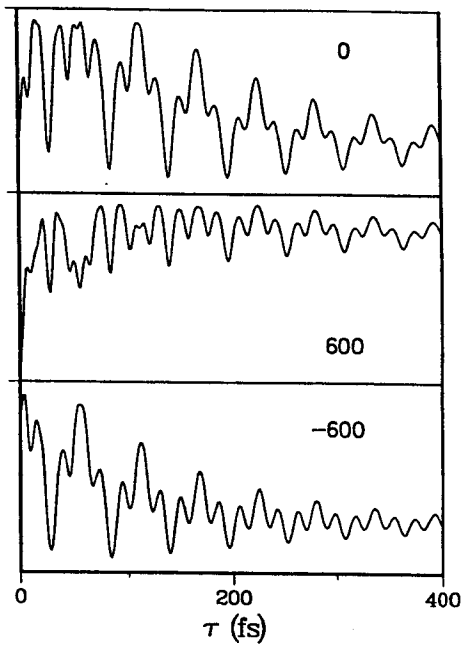

Figure 6 (*b*) The differential absorption signal detected at fixed ω_2 frequencies is displayed as a function of the time delay τ for the model system of Figure 6(*a*). Coherent vibrational motion of the Raman active modes is clearly seen. The detection frequencies are $\omega_2 - \omega_{eg} = 0$, 600 cm^{-1} and $-600\ \text{cm}^{-1}$ as indicated in each panel. The different traces are arbitrarily scaled.

$$S_{\text{HB}}(\tau;\omega_1,\omega_2) = \text{Re}\int_0^\infty dt' \exp[-i(\omega_2-\omega_1)t'] \times [\langle \mathcal{G}_{ge}(t')\mathcal{G}_{ee}(\tau)\mathcal{G}_{eg}(t')\rho_g\rangle + \langle \mathcal{G}_{ge}(t')\mathcal{G}_{gg}(\tau)\mathcal{G}_{eg}(t')\rho_g\rangle] \quad 25.$$

where the first term is $R_2(t_3,\tau,t_1)$ and the second term is $R_3(t_3,\tau,t_1)$ with $t_1 = t_3 = t'$. It was shown above that inhomogeneous broadening contributes to R_2 and R_3 a multiplicative factor of $\chi(t_3-t_1)$. Since the hole signal depends only on $t_1 = t_3 = t'$, inhomogeneous broadening is completely eliminated from the signal. The hole profile measured by tuning ω_2 with respect to ω_1 will thus contain narrow resonances, free of inhomogeneous broadening. If the nuclear dynamics timescale is very slow but finite, the line broadening is effectively inhomogeneous for short delay time τ; as τ increases the spectrum undergoes spectral diffusion and the

hole will broaden (36a–c, 65a–c, 69a,b). This is shown schematically in Figure 5.

Photon Echoes

Photon echo techniques (two pulse, stimulated, or accumulated echoes) provide an elegant means of eliminating inhomogeneous broadening (36a–c, 53, 74a–d). In the stimulated echo technique, the medium interacts with three external pulses with wavevectors $\mathbf{k}_1$, $\mathbf{k}_2$, and $\mathbf{k}_3$, centered at times $-(\tau'+\tau)$, $-\tau$, and 0 respectively. τ and τ' are the time intervals between the pulses. The signal is the scattered field with $\mathbf{k}_S = \mathbf{k}_3+\mathbf{k}_2-\mathbf{k}_1$ and is peaked at time $t = \tau'$ following the third pulse. The signal $S_{\rm PE}(\tau', \tau)$, which is defined as the total area of the echo pulse, is then detected as a function of τ' and τ. It is given by

$$S_{\rm PE}(\tau', \tau) = \int_0^\infty dt\, |P^{(3)}(\mathbf{k}_S, t)|^2. \qquad 26.$$

When the excitation pulses are short compared to molecular nuclear motions and the electronic dephasing, the echo signal is given by (72)

$$S_{\rm PE}(\tau', \tau) = \int_0^\infty dt\, |R_2(t, \tau, \tau')+R_3(t, \tau, \tau')|^2 |\chi(t-\tau')|^2. \qquad 27.$$

In Eq. 27, R_2 and R_3 are the nonlinear response functions of the optical medium in the absence of inhomogeneous broadening. The contribution of the inhomogeneous broadening is given by $\chi(t-\tau')$. For large inhomogeneous widths, the signal is sharply peaked around $t = \tau'$. This is why it is denoted an "echo." Following the third pulse, the echo appears after a delay τ'. Optical echo experiments normally use a slow detector and do not measure the echo as such, only its integrated intensity Eq. 26. The temporal resolution of the experiment is determined by the laser pulses that control τ and τ'. When the inhomogeneous broadening is large compared with other electronic dephasing, $\chi(t-\tau')$ is effectively a δ function. Substituting it in Eq. 27 and making use of Eqs. 5c, we get

$$S_{\rm PE}(\tau', \tau) = |\langle \mathscr{G}_{ge}(\tau')\mathscr{G}_{ee}(\tau)\mathscr{G}_{eg}(\tau')\rho_g\rangle + \langle \mathscr{G}_{ge}(\tau')\mathscr{G}_{gg}(\tau)\mathscr{G}_{eg}(\tau')\rho_g\rangle|^2. \qquad 28.$$

Equations 28 and 25 show that the stimulated echo is closely related to the hole-burning, since both depend on the same nuclear correlation function.

The ordinary photon echo is a two pulse technique in which the second and the third pulses are the same, $\mathbf{k}_2 = \mathbf{k}_3$. The signal appears at $\mathbf{k}_S = 2\mathbf{k}_2-\mathbf{k}_1$ and it is obtained from Eq. 28 by setting $\tau = 0$ (68a,b). The accumulated echo is another echo technique that uses a train of pulses. Its information content is identical to the stimulated echo. Figure 7 displays the ordinary echo signal for a three mode molecular system (72).

IMPULSIVE OFF RESONANT RAMAN SCATTERING AND QUANTUM BEATS

When $P^{(3)}$ is calculated by using Eq. 5, we find that it has various factors in which a single field frequency ω_j or a combination of two $\omega_j \pm \omega_k$ or three $\omega_j \pm \omega_k \pm \omega_m$ field frequencies is resonant with a molecular transition $\omega_{vv'}$. These factors originate from the t_1, the t_2, and the t_3 integrations and represent single photon, two photon, and three photon resonances, respectively. In the Raman process we are looking at *two photon* resonances whereby a difference in two field frequencies is resonant with a molecular vibrational transition, $\omega_1-\omega_2 = \omega_{vv'}$. The optical signal and its interpretation are greatly simplified when all of the light beams are tuned far off resonance from any electronic transition. In that case the photons do not

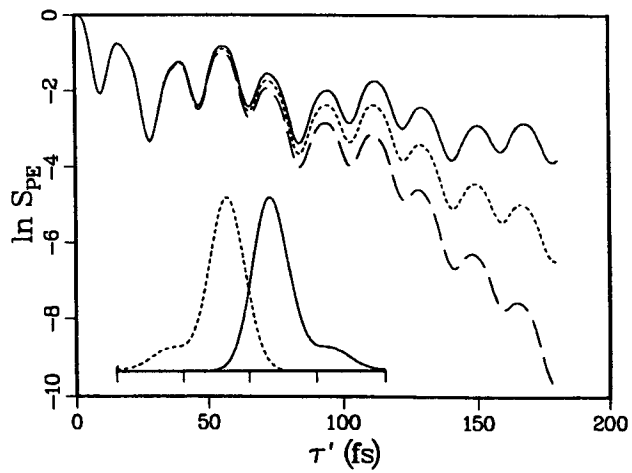

Figure 7 The impulsive two pulse echo (Eq. 28 with $\tau = 0$) for a three mode system with two coherent modes $\omega_1 = 600\ \text{cm}^{-1}$, $d_1 = 0.4$, $\omega_2 = 1800\ \text{cm}^{-1}$, $d_2 = 0.5$. In addition it has an overdamped mode with $\Delta_3 = 510\ \text{cm}^{-1}$. The *solid*, *dashed*, and *long dash curves* correspond to $\Lambda_3/\Delta_3 = 10^{-4}, 5\times10^{-4}$, and 10^{-3}, respectively. The linear absorption and the fluorescence lineshapes for this model are broad and structureless and virtually identical for the three values of Λ_3/Δ_3. The *inset* shows the linear absorption (*solid curve*) and fluorescence (*dotted curve*) for this system. The frequency scale is $2000\ \text{cm}^{-1}$ between ticks. The figure demonstrates the greater sensitivity of the photon echo to nuclear motions compared with linear spectroscopy.

get absorbed but are simply scattered. In terms of our response function, we expect the "particle" contribution to the spectrum to vanish, and the signal should reflect solely the "hole" dynamics in the ground state, as given by $\mathcal{G}_{gg}(t_2)$, because the excited state is never populated. The optical polarization $P^{(3)}$ is purely imaginary and varies as $(\omega_1-\omega_{eg})^{-2}$. When the laser frequencies are tuned near resonance we get additional single photon and three photon resonances, and the excited state "particle" dynamics, as given by $\mathcal{G}_{ee}(t_2)$, contributes as well. The experiment carries, in this case, more information and its interpretation is more complex. In this section, I analyze off resonant Raman spectroscopies. A proper description of off resonant scattering requires the incorporation of the dependence of the electronic dipole moment on the nuclear displacements. Thus the Condon approximation is not invoked in this section.

Spontaneous Raman

In ordinary (spontaneous) Raman spectroscopy (47b) a stationary light beam of frequency ω_1 is scattered off the molecular system. The scattered light has sharp resonances for frequencies ω_2 whenever $\omega_2-\omega_1=\omega_{x'x}$ where $\omega_{x'x}$ is a vibronic transition. The Raman process can be calculated by using the present response functions (47b). The intensity of the scattered light is given by

$$S_R(\omega_1-\omega_2)=\int_{-\infty}^{\infty} dt \exp[i(\omega_1-\omega_2)t]\langle\mu^2\mathcal{G}_{gg}(t)\mu^2\rho_g\rangle. \qquad 29.$$

Stationary Coherent Anti-Stokes Raman (CARS)

A coherent Raman process (47a–c, 75–76a–c) is a four wave mixing process that involves the interaction of molecules with two laser fields with wavevectors $\mathbf{k}_1$ and $\mathbf{k}_2$ and frequencies ω_1 ans ω_2, and that detects the coherently generated signal with $\mathbf{k}_S=2\mathbf{k}_1-\mathbf{k}_2$ and $\omega_S=2\omega_1-\omega_2$. Narrow Raman resonances are observed whenever the frequencies of the two fields differ by a ground state vibrational transition, $\omega_1-\omega_2=\omega_{x'x}$. The technique has a better sensitivity compared with the spontaneous Raman, due to the directionality (phase matching) of the signal. The CARS signal is given by,

$$S_{CARS}(\omega_1-\omega_2)=|P(2\mathbf{k}_1-\mathbf{k}_2)|^2 \qquad 30.$$

where

$$P(2\mathbf{k}_1-\mathbf{k}_2)=i\int_0^{\infty} dt \exp[i(\omega_1-\omega_2)t]\langle i[\mu^2(t),\mu^2(0)]\rho_g\rangle \qquad 31.$$

and

$$\langle i[\mu^2(t),\mu^2(0)]\rho_g\rangle = i[\langle\mu^2\mathcal{G}_{gg}(t)\mu^2\rho_g\rangle-\langle\mu^2\mathcal{G}_{gg}(t)\rho_g\mu^2\rangle]. \qquad 32.$$

If we expand the electronic dipole in the nuclear displacements (non-Condon contributions) $\mu\cong\mu_{eg}[1+\sum_j\kappa_j q_j]$, we get for the Brownian oscillator model (72)

$$\langle i[\mu^2(t),\mu^2(0)]\rho_g\rangle = 4|\mu_{eg}|^4\sum_j\frac{\kappa_j^2}{\omega_j}\dot{M}_j(t). \qquad 33.$$

Picosecond CARS Spectroscopy

In this technique (31a,b, 77–81), an initial simultaneous pair of picosecond pulses with wavevectors $\mathbf{k}_1$ and $\mathbf{k}_2$, prepares a coherent superposition of two vibrational states by stimulated Raman scattering. After a specified delay period, τ, a third pulse with wavevector $\mathbf{k}_1$ is scattered from the system, and the signal with wavevector $\mathbf{k}_S=2\mathbf{k}_1-\mathbf{k}_2$ is collected. Its variation with the relative delay τ is a measure of vibrational dephasing processes. The picosecond CARS can be viewed as a *transient grating* technique (33, 34a,b). The initial pulses prepare a moving grating with wavevector $\mathbf{k}_1-\mathbf{k}_2$ which oscillates at the frequency $\omega_1-\omega_2$. The second pulse is scattered from this grating and $\mathbf{k}_3=\mathbf{k}_1+(\mathbf{k}_1-\mathbf{k}_2)$ is simply the Bragg diffraction condition. This technique has been applied to the study of vibrational relaxation in liquids (31a,b, 80), molecular crystals (77, 78), and in molecular beams (79). Picosecond pulses are much longer than typical molecular vibrational periods. They may, however, be much shorter than the inverse linewidths of vibrational transitions. The picosecond CARS is, therefore, essentially a frequency domain experiment with respect to the molecular vibrations. By tuning $\omega_1-\omega_2$ to be equal to a particular vibronic frequency $\omega_{x'x}$ the CARS experiment selects a particular vibrational transition. The experiment is, however, time resolved with respect to the vibrational relaxation dynamics. Setting $\omega_1-\omega_2=\omega_{x'x}$, we get

$$S_{x'x}(\tau)=|\chi_{x'x}(\tau)|^2 \qquad 34a.$$

with $\chi_{x'x}(t)$ the component of the response function (Eq. 32) that oscillates at the $\omega_{x'x}$ frequency, i.e.

$$\chi_{x'x}(\tau)=i[\langle(\mu^2)_{xx'}\mathcal{G}_{gg}(\tau)(\mu^2)_{x'x}\rho_{xx}\rangle - \langle(\mu^2)_{xx'}\mathcal{G}_{gg}(\tau)\rho_{x'x'}(\mu^2)_{x'x}\rangle]\exp(-i\omega_{x'x}\tau). \qquad 34b.$$

Here $\rho_{xx}\equiv\langle x|\rho_g|x\rangle$ and $\mathcal{G}_{gg}(\tau)$ represents the dynamics of nuclear degrees of freedom, other than the Raman mode being probed.

Femtosecond CARS: Impulsive Stimulated Light Scattering (ISLS)

This technique, pioneered by Nelson, Ippen and coworkers (46a,b, 82a,b), is very similar to the picosecond CARS except that it uses shorter (femtosecond) pulses. These pulses are shorter than the vibrational periods being measured and are capable of probing molecular vibrations in real time. The signal is again observed at $2\mathbf{k}_2-\mathbf{k}_1$ and is given by $|P^{(3)}(\mathbf{k}_2,\tau)|^2$,

$$S_{\mathrm{ISLS}}(\tau)=|\chi_{\mathrm{ISLS}}(\tau)|^2 \qquad 35a.$$

with

$$\chi_{\mathrm{ISLS}}(\tau)=\int_{-\infty}^{\tau}d\tau_1|E(\tau_1)|^2\langle i[\mu^2,\mu^2(\tau-\tau_1)]\rho_g\rangle. \qquad 35b.$$

The signal depends on the same response function as stationary CARS (Eq. 32). Formally, the expressions are very similar to the picosecond CARS (47a–c, 83a,b), except that in the latter case the pulses, which have a narrower bandwidth, can select a given vibronic transition $\alpha'\alpha$ whereas in the femtosecond technique, which has lower spectral resolution, all states are accessible and the observed temporal pattern is very different. In an ideal impulsive experiment $|E(\tau_1)|^2$ is infinitely short and $\chi_{\mathrm{ISLS}}(\tau)$ is equal to the response function (Eq. 32). By properly shaping $|E(\tau)|^2$, it may become possible to excite selectively chosen modes. This was recently demonstrated in an impulsive Raman measurement performed by using a train of femtosecond pulses (28a–c).

The stationary, picosecond, and femtosecond CARS form a beautiful hierarchy. The stationary technique is a frequency domain technique in which the information on vibrational frequencies and relaxation is obtained by tuning the Raman frequency $\omega_1-\omega_2$. Picosecond CARS is frequency domain with respect to the molecular vibrations (i.e. we select a given transition by tuning the Raman frequency $\omega_1-\omega_2=\omega_{\alpha\alpha'}$). The vibrational relaxation and dephasing are observed, however, in the time domain by varying the delay time τ. The impulsive femtosecond Raman is purely time domain, and both the vibrational frequencies and their relaxation are observed through the oscillations and the damping of the time resolved beat pattern.

DISCUSSION

In this review I have discussed the analysis of ultrafast nonlinear optical spectroscopy using the density matrix. The density matrix can be calculated by using the vibronic eigenstates or the Wigner phase space representation,

which offers a simple semiclassical picture. The density matrix is a more complicated object than the wavefunction for the obvious reason that the dimensionality of phase space (which includes the coordinates $\mathbf{q}$ and momenta $\mathbf{p}$) is twice that of configuration space. However, it provides the most natural and overall the simplest description of nonlinear optical spectroscopy. Its advantages are apparent for large systems at finite temperatures. By propagating a density matrix representing a mixed state (rather than a pure state), we calculate directly the thermally averaged signal; no further averaging over thermal distributions is necessary. Furthermore, if we consider polyatomic molecules in condensed phases, we may develop a *reduced description* in which we follow explicitly only the dynamics of a few selected and relevant degrees of freedom. The remaining degrees of freedom are treated as a thermal bath using statistical methods. The bath can consist of some intramolecular vibrational degrees of freedom, which are weakly coupled to the electronic transition, solvent degrees of freedom, local modes for impurity spectra, etc. The density matrix provides a natural way for developing a reduced description. The Langevin equations for the Brownian oscillator model are an example of a simple reduced description. By contrast, wavefunction-based theories calculate a transition amplitude, and the signal is related to its absolute square. Statistical averaging can therefore be done only at the end of the calculation. The density matrix provides a unified computational scheme for isolated molecules, molecular clusters and condensed phase spectroscopy. The application of this procedure to complex systems with many nuclear degrees of freedom is straightforward.

The nonlinear response function is calculated by summing over the various possible pathways in Liouville space that lead to the final polarization as represented in the coupling scheme (Figure 1) or the double-sided Feynman diagrams (Figure 2). This calculation amounts to a *path integral in Liouville space*. Liouville space pathways are complex quantities, and they may interfere when added. This interference effect can be observed experimentally in certain cases and can be dramatic (42c, 75–76a–c). This type of path integral is different from, although conceptually similar to, the Feynman space-time path integrals. In recent years, path integrals have been extensively developed as a tool for numerical computations of liquid state properties (84a–d). In particular, a systematic mixed formulation in which some degrees of freedom (e.g. electronic) are quantum mechanical whereas others (e.g. nuclei) are treated classically is feasible. The present formulation strongly suggests a similar development for phase space based numerical procedures. The interpretation of nonlinear optical measurements in terms of dephasing processes, which is particularly useful for complex systems, is natural in the density matrix formulation. The non-

linear response function clarifies the relationships among different nonlinear spectroscopies that differ by the temporal sequences of pulses and by the choice frequencies and wavevectors. Pump-probe, fluorescence, Raman, four wave mixing, hole-burning, photon echoes, and transient gratings are thus treated in a compact and unified fashion. Furthermore, it can be shown that correlation functions and electronic dephasing rates, extracted from nonlinear optical measurements, may be directly used to calculate adiabatic, nonadiabatic, and superexchange electron transfer rates in the same solvent (85).

I now summarize the main points discussed in the review.

Snapshot Picture of Pump-Probe Spectroscopy

In an ideal pump-probe experiment, the laser pulses should satisfy three basic conditions: well separated pulses (WSP), pulses short compared with nuclear dynamics (PSN), and long compared with the electronic dephasing timescale (PLD). The last two conditions can be simultaneously satisfied provided the dephasing timescale (i.e. inverse linewidth) is much shorter than the timescales of the relevant motions probed as the time delay τ is varied. An example is the ICN photodissociation experiment in which the pump absorption linewidth of a few thousand cm^{-1} corresponds to a t_1 timescale of ~ 5 fsec. The relevant molecular dynamics (in this case the bond breaking) takes place in ~ 200 fsec. The probe absorption is broad only at short delay times (Figure 4*a*), and the fast dephasing condition clearly breaks at long delays where the lineshape narrows (Figure 4*c*). Another example is the solvent dielectric relaxation, as reflected in the time dependent Stokes shift. In solvated dyes, the absorption linewidth is typically ~ 500 cm^{-1}, which amounts to 60 fsec, whereas the dielectric relaxation is in the psec range. When this separation of timescales holds, we can use pulses that are long compared with the dephasing timescale and short compared with the relevant molecular dynamics. We can then describe the pump-probe experiment in terms of three stages: instantaneous preparation of a doorway state, an evolution period, and an instantaneous detection through the window state. This is the snapshot spectrum (Case I) in which the light pulses can be considered both spectrally narrow (compared with the dephasing rate) and temporally short (compared with the molecular dynamics timescale). The ability to control the delay time τ in Case I (and to a lesser extent in Case III) is the main advantage of the pump-probe technique. In steady state measurements, we integrate over all values of τ and the signal in many cases is mostly determined by the long times, making it insensitive to the short time dynamics.

If, in addition to the assumptions made in Case I, we make a classical

approximation for the doorway and the window states, we obtain Case IV. The present formulation clarifies the range of validity of the classical picture and the approximations made. It is clear that, although qualitatively correct, the classical picture has limitations. One of the most appealing aspects of the classical Condon approximation is that it allows the direct, back-of-the-envelope, inversion of experimental spectra to obtain the intermolecular potentials (26a,b). This may be done since in this approximation at every nuclear configuration the system absorbs only a single frequency. Our exact expressions for the doorway and the window function show the limitations of this procedure and point out practical ways for improvements by more rigorous calculation of the doorway and window functions. In Cases II and III the spectrum is obtained by convoluting the snapshot spectrum with the spectral or temporal profiles of the laser pulses, respectively. In these cases, the experiment can still be interpreted in terms of the snapshot spectrum. When the WSP condition holds (Cases I–V), the experiment can be viewed as linear optics of the nonequilibrium state prepared by the pump (the doorway state). In Cases VI and VII we lose this picture, and the experiment has to be treated as a single four wave mixing process since we can no longer separate it into three distinct stages.

Homogeneous and Inhomogeneous Broadening

Nonlinear spectroscopies provide more dynamical information than ordinary linear spectroscopic investigations of lineshapes. This is clearly seen by examining the corresponding response functions. The linear polarization $P^{(1)}$ is related to the average of a single propagation period $\langle \mathcal{G}(t_1) \rangle$, whereas $P^{(3)}$ is related to the average of a product of three evolution periods $\langle \mathcal{G}(t_3)\mathcal{G}(t_2)\mathcal{G}(t_1) \rangle$. When the nuclear coordinates are static, the latter average becomes a simple function $\chi(t_1 - t_3)$ for R_2 and R_3 and $\chi(t_1 + t_3)$ for R_1 and R_4. We denote this limit as inhomogeneous broadening. In the reverse limit, when the nuclear motions are very rapid we can factorize $\langle \mathcal{G}(t_3)\mathcal{G}(t_2)\mathcal{G}(t_1) \rangle \cong \langle \mathcal{G}(t_3) \rangle \langle \mathcal{G}(t_2) \rangle \langle \mathcal{G}(t_1) \rangle$. We denote this as homogeneous broadening. The overdamped Brownian oscillator model is an example that interpolates between the homogeneous (Eq. 22) and the inhomogeneous (Eq. 21) limits. In that model the homogeneous line is a Lorentzian and the inhomogeneous line is a Gaussian. This is, however, not necessarily always the case (73). The distinction between homogeneous and inhomogeneous broadening cannot be made by using the linear absorption and must be based on the multitime correlation functions and $\hat{S}^{(3)}$. By formulating nonlinear optics in terms of these correlation functions, we can classify the nonlinear techniques in a hierarchy depending on their information content. The early theoretical treatments of pico-

second CARS (31a,b, 86) led to the prediction that the spatial phase matching condition in these experiments allows them to selectively eliminate the inhomogeneous vibrational linewidth. It was later shown by Loring & Mukamel (81) that these predictions are incorrect, since the signal is described by a single Green function $\langle \mathcal{G}(t_1) \rangle$ and is simply given by the Fourier transform of the spontaneous Raman spectrum.

Quantum Beats

Several femtosecond spectroscopies (4, 5, 8–9a,b, 11–13) show simple damped harmonic oscillations with frequencies of only a few molecular vibrations. These quantum beats appear even in systems with a very large electronic dephasing in which the linear absorption is broad and structureless, and reflect the line narrowing capacity of these measurements. These observations raise many interesting questions: How does the experiment select a few vibrational modes? Do the beats represent ground state or excited state evolution? What is the role of coupling to the medium (homogeneous, inhomogeneous broadening and spectral diffusion processes) in these measurements? All these questions are simply answered by the formulation presented here. The photon echo and the hole-burning techniques eliminate inhomogeneous broadening, since they probe the average of quantities such as $\langle \mathcal{G}_{ge}(t_3)\mathcal{G}_{ee}(t_2)\mathcal{G}_{eg}(t_1) \rangle$ for $t_1 = t_3$. For inhomogeneous broadening this correlation function does not depend on t_2 and the inhomogeneous broadening in the t_1 and the t_3 periods simply cancels. The Raman spectroscopies show quantum beats for a different reason; in these techniques we probe $\langle \mathcal{G}_{gg}(t_2) \rangle$. This is the propagation of a ground state population that is not affected by electronic dephasing (whether homogeneous or inhomogeneous).

Fourier Transform Relationships

There are general Fourier transform relationships among frequency domain and time domain techniques. Such relationships have recently been utilized to conduct femtosecond measurements by using stationary stochastic light sources with an ultrashort coherence time (87–89). The question often arises as to whether the information derived from a particular femtosecond technique could be obtained by an equivalent frequency domain measurement. The nonlinear susceptibility $\chi^{(3)}$ describes the stationary response of the system to three monochromatic fields with frequencies ω_1, ω_2, and ω_3. $\chi^{(3)}$ can be obtained by performing a triple Fourier transform of $\hat{S}^{(3)}(t_3, t_2, t_1)$ over the three time variables (47a–c, 54–55a,b). Thus, there is an exact and general *triple Fourier transform* relationship between stationary and impulsive four wave mixing spectroscopies. In principle, if we conduct a complete set of stationary four wave

mixing experiments and measure $\chi^{(3)}$ for all possible values of ω_1, ω_2, and ω_3 we could obtain the impulsive response. An interesting practical question is whether there exists a *single Fourier transform* relationship among various techniques. This is true only in certain special cases of detuning and pulse durations, where two of the time variables in $\hat{S}^{(3)}$ are not important and the technique essentially probes a single propagation period. An exact relationship between the stimulated echo and hole-burning was established in Eqs. 25 and 28. The various Raman spectroscopies are also closely related. Upon comparing the stationary, spontaneous, and the coherent Raman signals, we note that the former is related to the *correlation function* of μ^2 and the latter to the *response function* of μ^2 (i.e. Eq. 32). The two are related by the fluctuation dissipation theorem (90)

$$\langle i[\mu^2(t), \mu^2(0)]\rho_g \rangle = \int_{-\infty}^{\infty} d\omega\, S_R(\omega)[1 - \exp(-\hbar\omega/k_B T)]\exp(-i\omega t). \quad 36.$$

For low temperatures $k_B T \ll \hbar\omega$ we can neglect the $\exp(-\hbar\omega/k_B T)$ factor and the two are simply related by a Fourier transform. Similarly the picosecond Raman signal is closely related to the spontaneous Raman. This may best be seen by expanding the spontaneous Raman correlation function in vibrational states

$$\langle \mu^2 \mathcal{G}_{gg}(t)\mu^2\rho_g \rangle = \sum_{\alpha,\alpha'} \langle (\mu^2)_{\alpha\alpha'} \mathcal{G}_{gg}(t)(\mu^2)_{\alpha'\alpha}\rho_{\alpha\alpha} \rangle \exp(-i\omega_{\alpha'\alpha}t), \quad 37.$$

where, as in Eq. 34b, $\mathcal{G}_{gg}(t)$ represents the dynamics of nuclear degrees of freedom other than the Raman mode being probed. The picosecond Raman technique selects a particular $\alpha'\alpha$ pair and, when the temperature is low compared with the vibrational frequency, the signal is related to the correlation function of $(\mu^2)_{\alpha\alpha'}$. The spontaneous Raman is thus simply the Fourier transform of the picosecond coherent Raman (81). Similarly, the amplitude for impulsive Raman scattering is the response function (Eq. 32), which is related to the Fourier transform of the stationary CARS.

ACKNOWLEDGMENTS

The support of the National Science Foundation, the Air Force Office of Scientific Research, and the Petroleum Research Fund, administered by the American Chemical Society, is gratefully acknowledged. It is a pleasure to thank Y. J. Yan, L. Fried, W. Bosma, and R. F. Loring for their invaluable contributions to the work covered in this review. The critical comments of D. Miller, J. Farrar, and A. Myers are most appreciated. Finally, I wish to thank R. Ferreri for the careful typing.

Literature Cited

1. Fork, R. L., Brito-Cruz, C. H., Becker, P. C., Shank, C. V. 1987. *Opt. Lett.* 12: 483
2. Yajima, T., Yoshihara, K., Harris, C. B., Shionoya, S., eds. 1988. *Ultrafast Phenomena VI*. Berlin: Springer-Verlag
3. Weiner, A. M., DeSilvestri, S., Ippen, E. P. 1985. *J. Opt. Soc. Am. B* 2: 654; Weiner, A. M., Ippen, E. P. 1985. *Chem. Phys. Lett.* 114: 456
4. Rosker, M. J., Wise, F. W., Tang, C. L. 1986. *Phys. Rev. Lett.* 57: 321; Wise, F. W., Rosker, M. J., Tang, C. L. 1987. *J. Chem. Phys.* 86: 2827
5. Walmsley, I. A., Wise, F. W., Tang, C. L. 1989. *Chem. Phys. Lett.* 154: 315
6. Becker, P. C., Fork, R. L., Brito-Cruz, C. H., Gordon, J. P., Shank, C. V. 1988. *Phys. Rev. Lett.* 60: 2462
7. Brito-Cruz, C. H., Fork, R. L., Knox, W. H., Shank, C. V. 1987. *Chem. Phys. Lett.* 132: 341

8a. Fragnito, H. L., Bigot, J. Y., Becker, P. C., Shank, C. V. 1989. *Chem. Phys. Lett.* 160: 101

8b. Becker, P. C., Fragnito, H. L., Bigot, J. Y., Brito-Cruz, C. H., Fork, R. L., Shank, C. V. 1989. *Phys. Rev. Lett.* 63: 505

9a. Chesnoy, J., Mokhtari, A. 1988. *Phys. Rev. A* 38: 3566; Mokhtari, A., Chesnoy, J. 1988. *Europhys. Lett.* 5: 523

9b. Mokhtari, A., Chesnoy, J., Laubereau, A. 1989. *Chem. Phys. Lett.* 155: 593

10a. Miller, R. J. D., Casalegno, R., Nelson, K. A., Fayer, M. D. 1982. *Chem. Phys.* 72: 371

10b. Nelson, K. A., Miller, R. J. D., Lutz, D. R., Fayer, M. D. 1982. *J. Appl. Phys.* 53: 1144

11a. Ruhman, S., Joly, A. G., Nelson, K. A. 1987. *J. Chem. Phys.* 86: 6563; Ruhman, S., Joly, A. G., Nelson, K. A. 1988. *IEEE J. Quantum Electron.* 24: 460

11b. Ruhman, S., Williams, L. R., Joly, A. G., Kohler, B., Nelson, K. A. 1987. *J. Phys. Chem.* 91: 2237

12a. Leonhardt, R., Holzapfel, W., Zinth, W., Kaiser, W. 1987. *Chem. Phys. Lett.* 133: 373

12b. Sellmeier, A., Scherer, P. O. J., Kaiser, W. 1984. *Chem. Phys. Lett.* 105: 140

12c. Gottfried, N. H., Sellmeier, A., Kaiser, W. 1984. *Chem. Phys. Lett.* 111: 326

13. Lotshaw, W. T., McMorrow, D., Kalpouzos, C., Kenney-Wallace, G. A. 1987. *Chem. Phys. Lett.* 136: 323; Kalpouzos, C., McMorrow, D., Lotshaw, W. T., Kenney-Wallace, G. A. 1989. *Chem. Phys. Lett.* 155: 240; 1988. *Chem. Phys. Lett.* 150: 138; McMorrow, D., Lotshaw, W. T., Kenney-Wallace, G. A. 1988. *IEEE J. Quantum Electron* QE-24: 443; Kalpouzos, C., McMorrow, D., Lotshaw, W. T., Kenney-Wallace, G. A. 1989. *Chem. Phys. Lett.* 155: 240; Kalpouzos, C., Lotshaw, W. T., McMorrow, D., Kenney-Wallace, G. A. 1987. *J. Phys. Chem.* 91: 2028

14a. Greene, B. I., Mueller, J. F., Orenstein, J., Rapkine, D. H., Schmitt-Rink, S., Thakur, M. 1989. *Phys. Rev. Lett.* 61: 325

14b. Greene, B. I., Orenstein, J. F., Millard, R. R., Williams, L. R. 1987. *Phys. Rev. Lett.* 58: 2750

15. Fann, W. S., Benson, S., Madey, J. M. J., Etemad, S., Baker, G. L., Kajzar, F. 1989. *Phys. Rev. Lett.* 62: 1492

16a. Fleming, G. R., Martin, J. L., Breton, J. 1988. *Nature* 333: 190

16b. Holzapfel, W., Finkele, U., Kaiser, W., Oesterhelt, D., Scheer, H., et al. 1989. *Chem. Phys. Lett.* 160: 1

17a. Genberg, L., Bao, Q., Gracewski, S., Miller, R. J. D. 1989. *Chem. Phys. Lett.* 131: 81

17b. Mathies, R. A., Brito-Cruz, C. H., Pollard, W. T., Shank, C. V. 1988. *Science* 240: 777

17c. Pollard, W. T., Lee, S. Y., Mathies, R. A. 1989. *J. Chem. Phys.* 92: 4012

18a. Robinson, M. M., Yan, Y. X., Gamble, E. B. Jr., Williams, L. R., Meth, J. S., Nelson, K. A. 1984. *Chem. Phys. Lett.* 112: 491

18b. DeSilvestri, S., Fujimoto, J. G., Ippen, E. P., Gamble, E. B. Jr., Williams, L. R., Nelson, K. A. 1985. *Chem. Phys. Lett.* 116: 146

18c. Williams, L. R., Nelson, K. A. 1987. *J. Chem. Phys.* 87: 7346

19a. Kasinski, J. J., Gomez-Jahn, L. A., Faran, K. J., Gracewski, S. M., Miller, R. J. D. 1989. *J. Chem. Phys.* 90: 1253

19b. Min, L., Miller, R. J. D. 1989. *Chem. Phys. Lett.* 163: 55

20a. Chemla, D. S., Schmitt-Rink, S., Miller, D. A. B. 1988. *Optical Nonlinearities in Semiconductors*, p. 83. New York: Academic

20b. Alivisatos, A. P., Harris, A. L., Levinos, N. J., Steigerwald, M. L., Brus, L. E. 1988. *J. Chem. Phys.* 89: 4001

20c. Wang, Y., Suna, A., Mahler, W., Kasowski, R. 1987. *J. Chem. Phys.* 87: 7315

21a. Oudar, J. L., Hulin, D., Migus, A., Antonetti, A., Alexandre, F. 1985. *Phys. Rev. Lett.* 55: 2074

21b. Knox, W. H., Chemla, D. S., Miller, D. A. B., Stark, J. B., Schmitt-Rink, S. 1989. *Phys. Rev. Lett.* 62: 1189

21c. Peyghambarian, N., Koch, S. W., Lindberg, M., Fluegel, B., Joffre, M. 1989. *Phys. Rev. Lett.* 62: 1185

22a. deBoer, S., Vink, K. J., Wiersma, D. A. 1987. *Chem. Phys. Lett.* 137: 99

22b. Wiersma, D. A., deBoer, S. 1988. See Ref. 2, p. 354

23. Kemnitz, K., Yoshihara, K., Tani, T. 1989. *J. Phys. Chem.* 93: 6704

24a. Migus, A., Gauduel, Y., Martin, J. L., Antonetti, A. 1987. *Phys. Rev. Lett.* 58: 1559

24b. Lu, H., Long, F. H., Bowman, R. M., Eisenthal, K. B. 1989. *J. Phys. Chem.* 93: 27

24c. Schnitker, J., Rossky, P. J. 1987. *J. Chem. Phys.* 86: 3462, 3471

25a. Rosker, M. J., Dantus, M., Zewail, A. H. 1988. *Science* 241: 1200

25b. Dantus, M., Rosker, M. J., Zewail, A. H. 1987. *J. Chem. Phys.* 87: 2395; 1988. *J. Chem. Phys.* 89: 6113, 6128

25c. Rose, T. S., Rosker, M. J., Zewail, A. H. 1988. *J. Chem. Phys.* 88: 6672

26a. Bersohn, R., Zewail, A. H. 1988. *Ber. Bunsenges. Phys. Chem.* 92: 373

26b. Bernstein, R. B., Zewail, A. H. 1989. *J. Chem. Phys.* 90: 829

27a. Misewich, J., Glownia, J. H., Rothenberg, J. E., Sorokin, P. P. 1988. *Chem. Phys. Lett.* 150: 374

27b. Glownia, J. H., Misewich, J. A., Sorokin, P. P. 1990. *J. Chem. Phys.* 92: 3335

28a. Weiner, A. M., Heritage, J. P., Kirschner, E. M. 1988. *J. Opt. Soc. Am. B* 5: 1563

28b. Weiner, A. M., Leaird, D. E., Wiederrecht, G. P., Nelson, K. A. 1990. *Science* 247: 1317

28c. Warren, W. S. 1988. *Science* 242: 878

29a. Kosloff, R., Rice, S. A., Gaspard, P., Tersigni, S., Tannor, D. J. 1989. *Chem. Phys.* 139: 201

29b. Brumer, P., Shapiro, M. 1986. *Chem. Phys. Lett.* 126: 541

30. Rabitz, H. 1988. *Atomic and Molecular Processes with Short Intense Laser Pulses*. New York: Plenum

31a. Laubereau, A., Kaiser, W. 1978. *Rev. Mod. Phys.* 50: 607

31b. Zinth, W., Nuss, M. C., Kaiser, W. 1984. *Phys. Rev. A* 30: 1139

32. Dick, B., Hochstrasser, R. M., Trommsdorff, H. P. 1987. In *Nonlinear Optical Properties of Organic Molecules and Crystals*, ed. D. S. Chemla, J. Zyss, p. 159. New York: Academic

33. Eichler, H. J., Günter, P., Pohl, D. W. 1986. *Laser-Induced Dynamic Gratings*. Berlin: Springer-Verlag

34a. Fayer, M. D. 1982. *Annu. Rev. Phys. Chem.* 33: 63

34b. Rose, T. S., Righini, R., Fayer, M. D. 1984. *Chem. Phys. Lett.* 106: 13

35. Wiersma, D. A., Duppen, K. 1987. *Science* 237: 1147

36a. Berg, M., Walsh, C. A., Narasimhare, L. R., Littau, K. A., Fayer, M. D. 1988. *J. Chem. Phys.* 88: 1564

36b. Gulotty, R. J., Walsh, C. A., Patterson, F. G., Wilson, W. L., Fayer, M. D. 1986. *Chem. Phys. Lett.* 125: 507

36c. Bai, Y. S., Fayer, M. D. 1989. *Phys. Rev. B* 39: 11066

37. Marcus, R. A. 1988. *Chem. Phys. Lett.* 152: 8

38. Williams, S. O., Imre, D. G. 1988. *J. Phys. Chem.* 92: 6648

39a. Engel, V., Metiu, H., Almeida, R., Marcus, R. A., Zewail, A. H. 1988. *Chem. Phys. Lett.* 152: 1

39b. Engel, V., Metiu, H. 1989. *J. Chem. Phys.* 90: 6116

40a. Choi, S. E., Light, J. C. 1989. *J. Chem. Phys.* 90: 2593

40b. Fain, B., Lin, S. H., Hamer, N. 1989. *J. Chem. Phys.* 91: 4485

41. Lee, S.-Y., Pollard, W. T., Mathies, R. A. 1989. *J. Chem. Phys.* 90: 6146

42a. Stock, G., Domeke, W. 1988. *Chem. Phys.* 124: 227

42b. Stock, G., Schneider, R., Domeke, W. 1989. *Chem. Phys.* 90: 7184

43. Benjamin, I., Wilson, K. R. 1989. *J. Chem. Phys.* 90: 4176

44a. Mitsunaga, M., Tang, C. L. 1987. *Phys. Rev. A* 35: 1720

44b. Walmsley, I. A., Mitsunaga, M., Tang, C. L. 1988. *Phys. Rev. A* 38: 4681

45. Walsh, A. M., Loring, R. F. 1989. *Chem. Phys. Lett.* 160: 299

46a. Yan, Y. X., Cheng, L. T., Nelson, K. A. 1988. *Advances in Nonlinear Spectroscopy*, ed. R. J. H. Clark, R. E. Hester, p. 299. New York: Wiley

46b. Nelson, K. A., Ippen, E. P. 1989. *Adv. Chem. Phys.* 75: 1

47a. Mukamel, S. 1982. *Phys. Rep.* 93: 1

47b. Mukamel, S. 1988. *Adv. Chem. Phys.* 70: 165

47c. Mukamel, S., Loring, R. F. 1986. *J. Opt. Soc. Am. B* 3: 595

48. Yan, Y. J., Fried, L. E., Mukamel, S. 1989. *J. Phys. Chem.* 93: 8149

49. Yan, Y. J., Mukamel, S. 1990. *Phys. Rev. A*. In press

50. Yan, Y. J., Mukamel, S. 1988. *J. Chem. Phys.* 88: 5735; 1988. *J. Chem. Phys.* 89: 5160

51. Jankowiak, R., Small, G. J. 1987. *Science* 237: 618

52. Volker, S. 1989. *Annu. Rev. Phys. Chem.* 40: 499

53. Hesselink, W. H., Wiersma, D. A. 1979.